ISSN 2070-0482, Mathematical Models and Computer Simulations, 2023, Vol. 15, No. 2, pp. 277–288. © Pleiades Publishing, Ltd., 2023.
Russian Text © The Author(s), 2022, published in Matematicheskoe Modelirovanie, 2022, Vol. 34, No. 9, pp. 54–70.

Simulation of Vortex Interaction with a Shock Wave for Testing Numerical Algorithms

M. A. Kirushina[a,]*, T. G. Elizarova[a], and A. S. Epikhin[b]

[a] *Keldysh Institute of Applied Mathematics, Russian Academy of Sciences, Moscow, Russia*

[b] *Ivannikov Institute for System Programming, Russian Academy of Sciences, Moscow, Russia*

**e-mail: m_ist@mail.ru*

Received April 12, 22; revised June 2, 2022; accepted June 27, 2022

Abstract—The results of numerical simulation of the problem of the interaction of a vortex flow with a shock wave are presented on the example of using a quasi-gas dynamic (QGD) numerical algorithm, which is implemented as the QGDFoam solver. The algorithm is based on regularized equations of gas dynamics. The algorithm is implemented in the OpenFOAM open software package. The results are compared with the published data obtained based on the Godunov type method of a high order of accuracy and variants of the Kurganov–Tadmor method included in the open software package.

Keywords: control volume method, OpenFOAM package, quasi-gas dynamic algorithm, nonstationary supersonic ideal gas flow

DOI: 10.1134/S2070048223020072

INTRODUCTION

Testing numerical methods for modeling gas-dynamic flows remains relevant due to the wide range of available numerical algorithms and the ever-expanding scope of these algorithms in practical calculations. Moreover, studying the possibilities of algorithms for describing unsteady flows is of particular importance. In this paper, the capabilities of four well-known algorithms for modeling inviscid flows are shown in the widespread problem of the development of an unsteady flow of an ideal gas, which is formed during the interaction of a moving vortex formation with a shock wave. The formulation of this problem and examples of modeling it based on schemes of a higher order of accuracy are given in a number of works, among which we note [1, 2] and refer to them as the reference ones. Each algorithm introduces its own characteristics in the results of numerical simulation, whose role can only be estimated from general considerations due to the lack of an analytical solution of the problem or experimental data on it. Nevertheless, a comparison of the results of modeling this complex flow, obtained based on various numerical approaches, makes it possible to reveal the features of the applied methods.

In this paper, on the example of mathematical modeling of this problem, the features of a quasi-gas dynamic (QGD) algorithm are analyzed, together with three other computational approaches based on the Kurganov–Tadmor scheme with second and first order of accuracy limiters.

Our attention is focused on the results of the calculations obtained based on the QGD algorithm [3, 4], which is included in the open package OpenFOAM [5] as a QGDFoam solver. The calculations were carried out in this package. The QGD algorithm is a difference approximation of the averaged equations of gas dynamics [3]. The QGD algorithm has a number of tuning parameters, an adequate choice of which makes it possible to uniformly model a wide range of gas flows, including both supersonic and subsonic modes. The dependence of the numerical solution on the choice of tuning parameters of the algorithm is shown.

A detailed description of the problem statement is given in the first section of the study. In the second part, the form of the QGD equations and the problem statement are given. Some features of the implementation of numerical algorithms and running the problem within the open package are described in the third section. The fourth section shows the results of calculations, their grid convergence, and the effect of the choice of the tuning parameters of the QGD algorithm. Here the results are obtained based on the three computational methods included in the open package OpenFOAM as alternative computational

cores. In conclusion, the obtained results are discussed and the speed efficiency of the algorithms used in an open software package are compared.

PROBLEM STATEMENT

The general view of the flow under study at the final moment of the calculation time and the scheme of the computational domain are shown in Figs. 1 and 2 in accordance with the works [1, 2].

The computational area has the form of a rectangle of size 2×1 (Fig. 1). At the initial moment of time, a stationary shock wave with the Mach number M_s is located vertically along the line with coordinate $x = 0.5$, in front of which there is a region of vortex flow with counterclockwise rotation of the velocity. In the left part of the region, the flow is a superposition of supersonic and vortex flows. Behind the shock wave there is a zone of subsonic flow.

The gas parameters to the left of the shock wave are indicated by index u (up); and on the right, by index d (down). The components of the flow velocity are denoted by the symbols (u, v).

The initial conditions on the left side of the area $x \le 0.5$ and the boundary conditions on the left boundary (upstream) have the form

$$\rho_u = 1, \quad u_u = M_s\sqrt{\gamma}, \quad v_u = 0, \quad p_u = 1, \quad T_u = p_u/(\rho_u R). \tag{1}$$

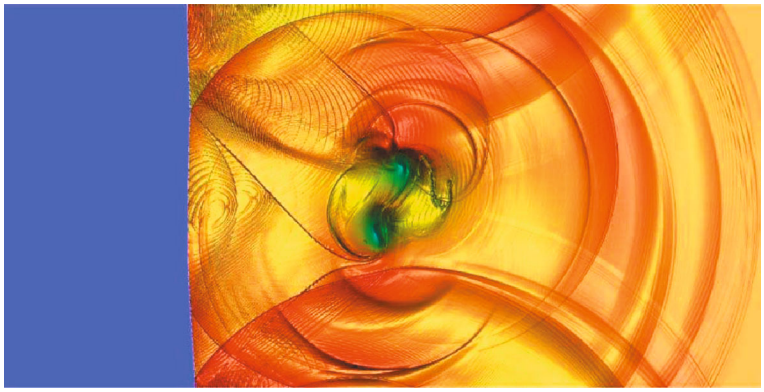

Fig. 1. An example of a flow pattern in the problem of inviscid interaction between a vortex and a shock wave according to [2].

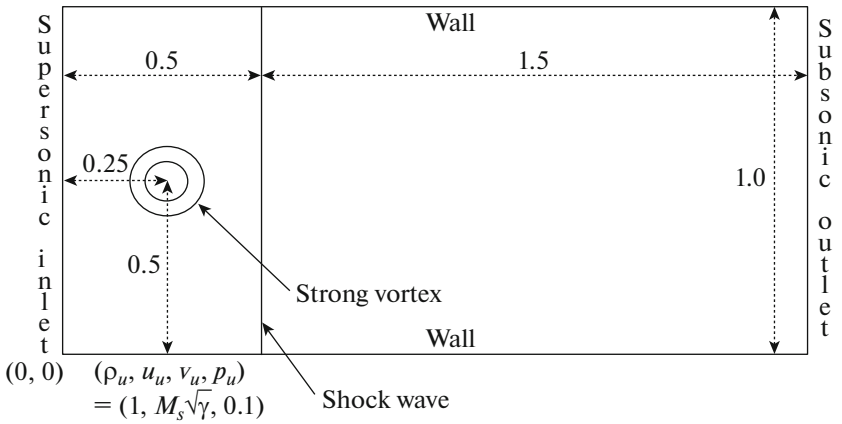

Fig. 2. Scheme of the computational domain and the initial conditions.

On the right side, the conditions are specified to ensure a stationary shock wave is specified in accordance with the Hugoniot conditions for the Mach number M_s. This corresponds to the parameters of the gas

$$\begin{gathered}\rho_d = \rho_u(\gamma+1)M_s^2/(2.0+(\gamma-1)M_s^2),\\ u_d = u_u(2.0+(\gamma-1)M_s^2)/((\gamma+1)M_s^2),\\ v_d = 0, \quad p_d = p_u(1+2\gamma(M_s^2-1)/(\gamma+1)), \quad T_d = p_d/(\rho_d R).\end{gathered} \tag{2}$$

In this task, we have chosen $M_s = 1.5$. Mach number in combination with the adiabatic index of a polytropic gas $\gamma = 1.4$ and the value of the gas constant $R = 1$ determines the values of the parameters in front of the shock wave and on the left boundary of the region, as well as the initial conditions for the calculation behind the shock wave. The numerical values of these quantities are

$$\rho_u = 1, \quad u_u = 1.77482, \quad v_u = 0, \quad p_u = 1, \quad T_u = 1,$$

$$\rho_d = 1.862, \quad u_d = 0.953146, \quad v_d = 0, \quad p_d = 2.45833, \quad T_d = 1.32022.$$

Note that in order to obtain a stationary shock wave in the calculation, the values of the parameters to the right of the discontinuity must be calculated sufficiently accurately. When applying the QGD algorithm, the minimum accuracy involves ten significant digits.

At the initial moment of time, a vortex formation is located in front of the shock wave with the center of the vortex at the point (0.25,0.5) with the inner radius $a = 0.075$ and outer radius $b = 0.175$. The values $M_v = 0.9$ and $v_m = M_v\sqrt{\gamma}$ are the additional characteristic parameters of the vortex.

We denote the velocity field inside the vortex as $(u^x_{\text{vor}}, u^y_{\text{vor}})$. The angular velocity is given as follows:

$$v_\theta(r) = \begin{cases} v_1 = v_m r/a, & r \leqslant a,\\ v_2 = v_m a/(a^2-b^2)(r-b^2/r), & a < r \leqslant b\\ 0, & r > b.\end{cases}$$

Then, $u^x_{\text{vor}}(r) = u_u - v_\theta(r)\sin\theta$ and $v^y_{\text{vor}}(r) = v_u + v_\theta(r)\cos\theta$.

The temperature inside the vortex is found by calculating the integral

$$\int_r^b \frac{dT_{\text{vor}}(r)}{dr}dr = \int_r^b \frac{\gamma-1}{R\gamma}\frac{v_\theta(r)^2}{r}dr,$$

where

$$\int_r^b \frac{\gamma-1}{R\gamma}\frac{v_\theta^2}{r}dr = \frac{\gamma-1}{R\gamma}\begin{cases}\displaystyle\int_r^a \frac{v_1^2}{r}dr + \int_a^b \frac{v_2^2}{r}dr, & r \leqslant a,\\ \displaystyle\int_r^b \frac{v_2^2}{r}dr, & a < r \leqslant b,\\ 0, & r > b.\end{cases}$$

Calculating the intergals, we find

$$T_{\text{vor}}(r) = \begin{cases} T_{\text{vor}}(b) - \dfrac{\gamma-1}{R\gamma}\dfrac{v_m^2}{a^2}\left(\dfrac{a^2-r^2}{2}\right)\\ -\dfrac{\gamma-1}{R\gamma}v_m^2\dfrac{a^2}{(a^2-b^2)^2}\left(\dfrac{b^2-a^2}{2} - 2b^2\ln\dfrac{b}{a} - \dfrac{b^4}{2}\left(\dfrac{1}{b^2}-\dfrac{1}{a^2}\right)\right), & r \leqslant a,\\ T_{\text{vor}}(b) - \dfrac{\gamma-1}{R\gamma}v_m^2\dfrac{a^2}{(a^2-b^2)^2}\left(\dfrac{b^2-r^2}{2} - 2b^2\ln\dfrac{b}{r} - \dfrac{b^4}{2}\left(\dfrac{1}{b^2}-\dfrac{1}{r^2}\right)\right), & a < r \leqslant b,\\ 0, & r > b,\end{cases}$$

using the fact that $T_{\text{vor}}(b) = T_u$. The pressure in the vortex p_{vor} is calculated as

$$p_{\text{vor}}(r) = p_u \left(T_{\text{vor}}(r)/T_u\right)^{\gamma/(\gamma-1)}.$$

The density ρ_{vor} in the vortex zone is determined from the equation of state. In the left part of the region in the vortex zone, the superposition of the values of velocities, temperatures, and pressures of the supersonic flow with the parameters of the inlet boundary is set as the initial conditions: values (1) are specified in the zone outside the vortex and the following values are specified in the zone inside the vortex:

$$\rho = \rho_{\text{vor}}, \quad u = u_{\text{vor}} = u_u - v_\theta(r)\sin\theta, \quad v = v_{\text{vor}} = v_\theta(r)\cos\theta, \quad p = p_{\text{vor}}, \quad T = T_{\text{vor}}(r).$$

In the right part of the region, the flow with the calculated parameters behind the shock wave (2) is specified.

The boundary conditions on the left boundary of the region are assumed to be constant, soft boundary conditions are set on the right boundary of the region, and the horizontal walls are assumed to be rigid boundaries with slip conditions for the velocity.

NUMERICAL ALGORITHM BASED ON REGULARIZED EQUATIONS

The system of regularized gas dynamic equations in the form of mass, momentum, and the total energy balance equations in the notation adopted in OpenFOAM is as follows:

$$\begin{gathered}
\partial_t \rho + \operatorname{div}(\mathbf{j_m}) = 0, \\
\partial_t(\rho\mathbf{u}) + \operatorname{div}(\mathbf{j_m}\mathbf{u}) + \nabla p = \operatorname{div}\hat{\Pi}, \\
\partial_t(\rho e) + \operatorname{div}[\mathbf{j_m}(e + p/\rho)] + \operatorname{div}\mathbf{q} = \operatorname{div}(\hat{\Pi}\mathbf{u}), \\
\mathbf{j_m} = \rho(\mathbf{u} - \mathbf{w}), \quad \mathbf{w} = \frac{\tau}{\rho}\left(\operatorname{div}(\rho\mathbf{u}\otimes\mathbf{u}) + \nabla p\right), \\
\hat{\Pi} = \hat{\Pi}_{NS} + \tau\mathbf{u}\otimes\left(\rho(\mathbf{u}\cdot\nabla)\mathbf{u} + \nabla p\right) + \tau\hat{I}\left((\mathbf{u}\cdot\nabla)p + \gamma p\nabla\mathbf{u}\right), \\
\mathbf{q} = \mathbf{q}_{NS} - \tau\rho\mathbf{u}\left((\mathbf{u}\cdot\nabla)u_\varepsilon + p(\mathbf{u}\cdot\nabla)/\rho\right).
\end{gathered} \tag{4}$$

Here, the specific total energy is denoted as $e = u_\varepsilon + 0.5|\mathbf{u}|^2$, u_ε is the specific internal energy, $p = \rho u_\varepsilon(\gamma - 1)$, and $T = p/\rho R$ is the temperature. The sign $\otimes$ denotes the direct tensor product of vectors and $\hat{I}$ is the unit tensor.

The mass flow vector, viscous stress tensor $\hat{\Pi}$, and the heat flux vector $\mathbf{q}$ are the traditional values supplemented by regularizing additions with a small coefficient τ as a multiplier. In this case, the values of the viscosity tensors and the heat flux vector, determined by the Newton and Fourier laws, are calculated as

$$\begin{gathered}
\hat{\Pi}_{NS} = \mu\left((\nabla\otimes\mathbf{u}) + (\nabla\otimes\mathbf{u})^T - \frac{2}{3}\hat{I}\operatorname{div}\mathbf{u}\right), \\
\mathbf{q}_{NS} = -\kappa\nabla T,
\end{gathered} \tag{5}$$

where $\mu = \mu(\rho, T) > 0$ is the coefficient of dynamic viscosity, $\kappa = \mu\gamma R/((\gamma - 1)\,\mathrm{Pr})$ is the coefficient of thermal conductivity, and Pr is the Prandtl number.

The system of QGD equations (4) includes an additional artificial dissipation, which ensures the stability and accuracy of the difference algorithm. This algorithm is explicit in time and uses the finite volume method with the approximation of all spatial derivatives of the second order of accuracy using central differences; see [3, 5]. The contribution of artificial dissipation is controlled by the coefficient

$$\tau = \alpha\Delta x/c.$$

Here Δx is the local step size of the spatial grid, c is the local speed of sound, and α is the tuning parameter of the algorithm, which usually lies within $0 < \alpha < 1$ and determines the accuracy of the algorithm and the time step of the explicit calculation scheme.

When solving the Euler equations based on the QGD algorithms, the dynamic viscosity coefficient and the related thermal conductivity coefficient are considered artificial. The viscosity coefficient is calculated as

$$\mu = \mu^{\text{QGD}} = p\tau\mathrm{Sc}^{\text{QGD}} \quad \text{and } \mathrm{Sc}^{\text{QGD}} \text{ is the Schmidt number.}$$

Thus, for this problem, all dissipative coefficients τ, μ, and κ are considered as artificial parameters that control the amount of introduced dissipation. The algorithm has three tuning parameters: numerical coefficients α, Sc^{QGD}, and Pr^{QGD}. Further, we will refer to Sc^{QGD} and Pr^{QGD} as Sc and Pr. In all further calculations, only the first two among them vary and the coefficient Pr is assumed to be one. As the practice of calculations shows, the effect of this parameter on the results is insignificant at values $Pr \sim 1$.

The boundary conditions for system (4) are set as follows: the specified conditions for the incoming flow (1) are maintained at the inlet boundary

$$u = u_u, \quad v = 0, \quad p = p_u, \quad T = T_u,$$

and at the outlet—the right boundary—mild drift conditions are used in the form of zero derivatives with respect to x for all gas-dynamic quantities. Special subsonic conditions do not apply. On the upper and lower boundaries of the region, the wall conditions with sliding are maintained; i.e.,

$$\partial u/\partial y = 0, \quad v = 0, \quad \partial T/\partial y = 0, \quad \partial p/\partial y = 0.$$

The problem is calculated up to dimensionless time $t = 0.7$.

FEATURES OF IMPLEMENTATION IN THE OpenFOAM PACKAGE

Numerical modeling in the OpenFOAM package involves the use of all quantities in a dimensional form in the C unit system. In the problem under consideration, the initial quantities according to [1, 2] are given in dimensionless form. To translate them into a dimensional form, we take into account that $R = 1$; hence, the value $C_p = \gamma R/(\gamma - 1) = 3.5$ and $R = R^*/M$, where R^* is the universal gas constant; and hence, the value of the molar mass of the gas is chosen in the form $M = 8314$ g/mol.

The dimensional values for this problem are given in Table 1.

Setting the conditions on the boundaries of the calculation area is given in Table 2.

The OpenFOAM program implements a three-dimensional flow; hence, its three components are specified in the velocity column. The computational grid and initial conditions are specified in the dictionaries of the OpenFOAM package. The value of the parameters of algorithm α and Sc is set in the QGD section of the thermophysicalProperties dictionary of the constant folder.

The results of calculations using QGDFoam were compared with the data obtained based on the computational core with the rhoCentralFoam solver. This solver is used to calculate compressible flows and is based on the so-called central-difference Kurganov schemes, which are versions of Godunov-type schemes with an increased order of accuracy [6]. For the rhoCentralFoam solver, various constraint options $\psi(r)$ were used, whose form depends on the gradient of the function V in two adjacent grid cells [7], where the argument of function r is calculated as

$$r = \left(V_p^n - V_{p-1}^n\right)\Big/\left(V_{p+1}^n - V_p^n\right).$$

Table 1. Gas parameters in dimensional form

Unit	Value
Molar mass M	8.314 kg/mol
Gas constant R	1 J/(kg K)
Adiabatic exponent γ	1.4
Heat capacity at constant pressure C_p	3.5 J/(kg K)

Table 2. Boundary conditions

	Inlet	Outlet	Walls
p	1	ZeroGradient	ZeroGradient
U	(1.7748 0.0 0.0)	ZeroGradient	Slip
T	1	ZeroGradient	ZeroGradient

In the first case, the VanLeer scheme, which has the 2nd order of approximation, is used, while the limiter used is $\psi(r) = (r + |r|)/(1 + |r|)$; in the second case, the minmod scheme, which has the first order of approximation, is used, with $\psi(r) = \max(\min(r,1),0)$; in the third case, the upwind scheme of the first order is used; in this case, the limiter is not used and it is assumed $r = 0$.

The way to interpolate values from the center of a cell to its edge is described in the fvSchemes dictionary in the interpolationSchemes section. All solvers used in the calculations were written in a form adapted for solving the Euler equations.

CALCULATION RESULTS

In the numerical simulation of the flow evolution, complex gas-dynamic configurations are formed with the appearance of various kinds of instabilities, which are both physical and computational in nature. In the flow, in particular, the Kelvin–Helmholtz instability can occur in the shock wave curvature zone, which is caused by the interaction of the vortex formation with it. Such instabilities have an inviscid nature and must be described in terms of the Euler equations in a two-dimensional consideration. The presence of viscous effects in the computational model can cause the formation of a viscous instability, for example, Tollmien–Schlichting waves. All these features of the flow are accompanied by acoustic effects. It is difficult to distinguish between the physical and computational nature of the instabilities. Algorithms using flow limiters, in addition to artificial ones, can also exclude physically justified fluctuations.

In [1], variants of the Godunov method of a higher order of accuracy are used with their adaptation to solve the problem. Instabilities are suppressed by introducing additional artificial dissipation, which replaces the dynamic viscosity coefficient in the terms Π_{NS} by the nonlinear coefficient proportional to the square of the spatial grid step. The details of this algorithm and the features of its software implementation on the example of one-dimensional and two-dimensional problems are additionally given in [8]. The algorithm [1] was adapted in a special way to the problem of the interaction of a vortex with a shock wave. In particular, to construct the reference solution on a grid with steps $h = 1/1200$, the velocities before and after the shock wave were recalculated in a special way to ensure the immobility of the shock wave and to avoid computational problems related to the calculation of a slowly moving shock.

In the QGD algorithm, the stability of the calculation is ensured by the τ-terms. Additional oscillation suppression is controlled by the Schmidt number Sc, which is included in the artificial dissipation coefficient μ^{QGD} and may vary. Note that all artificial dissipative terms are proportional to the spacing of the spatial grid. The latter makes the QGD algorithm a method of first order approximation in space, while all spatial derivatives are approximated with the second order of accuracy.

In our calculations, we used a sequence of condensing grids with square cells 1/400, 1/800, and 1/1600 in size.

Calculations were made on a hybrid K-100 computing cluster (https://www.kiam.ru/MVS/resources/k100.html). One to 36 processors were used.

The calculation results are presented in the form of density gradient fields. The figures show the fields of Schlieren values, which, in accordance with [1], is calculated as $\mathrm{Sch} = \ln(1 + \|\nabla\rho\|)/\ln(10)$ with limits of the value change in the range (0.1–2.0 or 2.4).

CALCULATIONS USING THE QGD ALGORITHM

Development of the flow at successive time moments $t = 0.1$, 0.2, 0.3, 0.4, 0.5, 0.6, and 0.7 is shown in Fig. 3 with the calculation parameters $\alpha = 0.5$ and $\mathrm{Sc} = 0$ on the coarsest grid with the spatial step $h = 1/400$. It can be seen from the sequence of figures that by the time $t = 0.3$ the vortex passes through the standing shock wave, distorting its profile. By the time $t = 0.5$, the shock wave profile returns to a state close to the initial one. Numerous interactions of reflected shocks and shock waves are seen. For a comparison time of 0.7, the center of the vortex is at the point (1.02, 0.49).

Figure 4 shows the calculations with the search for the closest solution to the reference [1] solution, which clarify the effect of the dissipative coefficients α and Sc. The calculations were carried out on a grid with step $h = 1/1600$. The best result (bottom figure) was obtained for the values $\alpha = 0.1$ and $\mathrm{Sc} = 0.1$. It shows the characteristic separation of the density into two parts in the center of the vortex and more distinct shock waves near the walls and at the outlet on the right than in the two upper figures. When calculating with $\alpha = 0.2$ and $\mathrm{Sc} = 1.0$, the center of the vortex appears to be less prominent. When calculating with $\alpha = 0.2$ and $\mathrm{Sc} = 0$, the center of the vortex almost coincides with the best calculation, but the shock

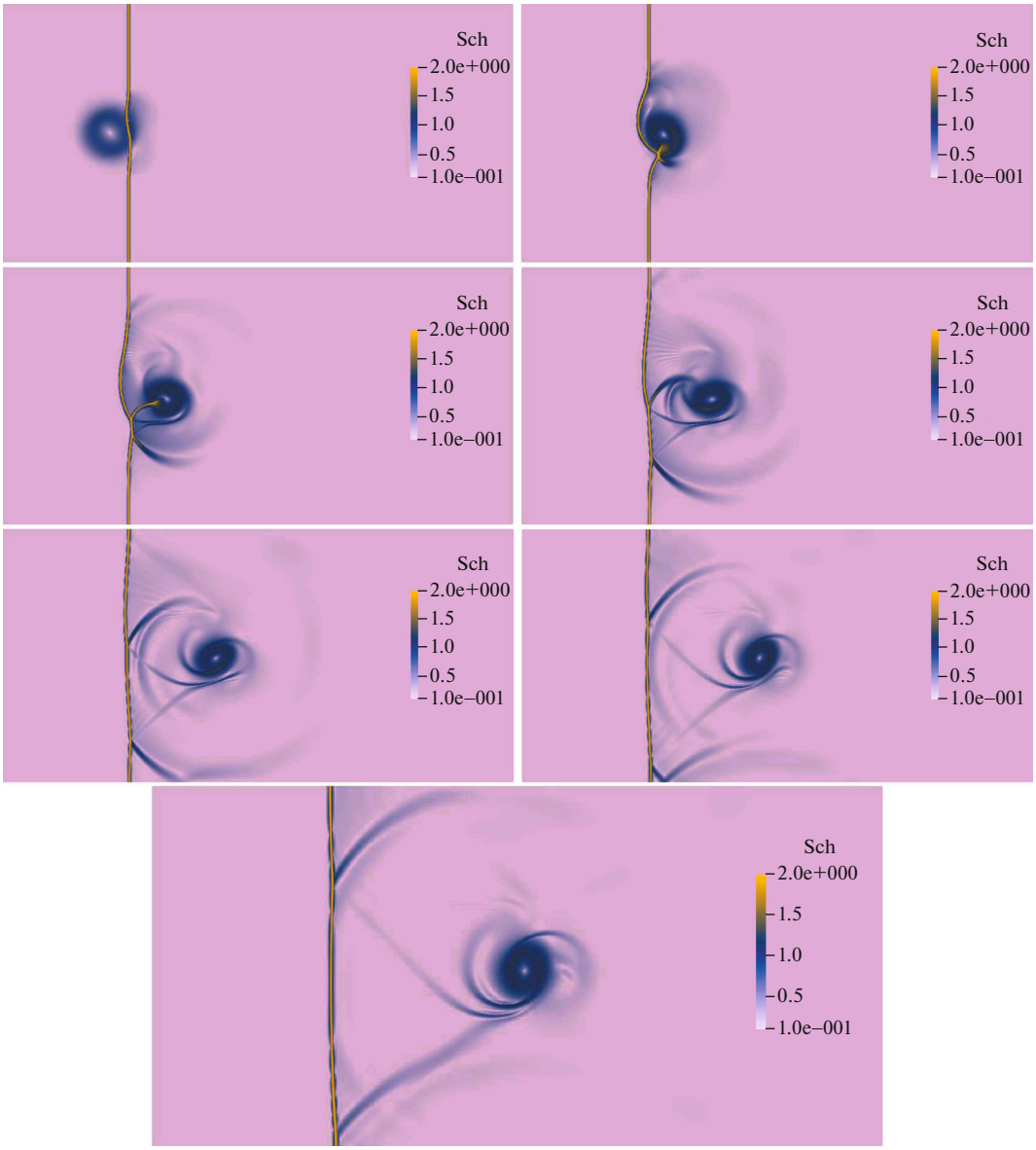

Fig. 3. Flow development (Schlieren), from left to right, with $t = 0.1, 0.2, 0.3, 0.4, 0.5, 0.6, 0.7$. Grid $h = 1/400$, $\alpha = 0.5$, $\mathrm{Sc} = 0$.

waves appear more blurred. If necessary, it is possible to fine-tune the dissipative coefficients, in particular, to use the values of the dissipative coefficients that depend on the local values of the gas-dynamic fields.

The presented pictures show that the variation of dissipative coefficients makes it possible to suppress the oscillations arising in a gas-dynamic flow with varying degrees of efficiency. Thus, the user can explicitly control this process and ensure that nonphysical oscillations are suppressed and that oscillations of the solution, which are of a physical nature, are preserved.

For a quantitative comparison of the calculations, the figures below show the density distributions along two selected vertical lines. These lines are selected in accordance with [1] (line *3*, $x = 0.52$) and [2] (line *5*, $x = 1.65$). To compare the results along line *3*, the reference data are given from [1]; and along line *5*, from [2].

Figure 5 shows the grid convergence for density ρ along lines *3* and *5* at $\alpha = 0.2$ and $\mathrm{Sc} = 0$. The distributions for grids with steps $h = 1/400$, $1/800$, and $1/1600$ are given. The plots demonstrate the monotonic convergence of the solution as the spatial mesh is thickened.

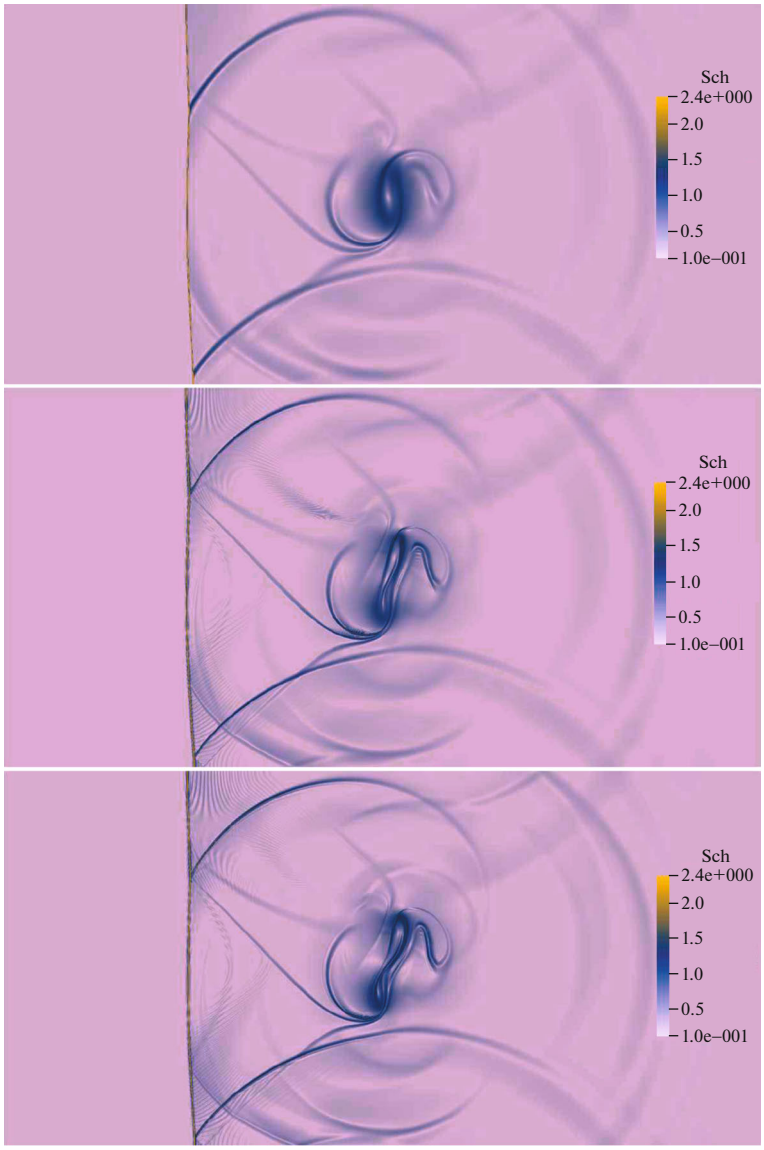

Fig. 4. $t = 0.7$. Grid $h = 1/1600$, from top to bottom: $\alpha = 0.2$, Sc = 1.0; $\alpha = 0.2$, Sc = 0; $\alpha = 0.1$, Sc = 0.1.

Figure 6 shows the dependence of the numerical solution of the problem on the value of the smoothing parameter α for density ρ along the same lines on the grid $h = 1/400$ at Sc = 0. Both graphs show the convergence of the solution as the dissipation parameter decreases. In this case, for line *3*, the value $\alpha = 0.1$ turns out to be insufficient to suppress the oscillations behind the shock wave. At the same time, line *5* is located in the zone of a fairly smooth solution, and in this zone, the dissipation coefficient can be reduced to 0.05.

CALCULATIONS USING VARIANTS OF THE rhoCentralFoam SOLVER

Figure 7 shows the calculations at time $t = 0.7$ for the original mesh $h = 1/400$. The calculations with the QGDFoam solvers $\alpha = 0.5$ and Sc = 0 are compared with three variants of the rhoCentralFoam solver using upwind, minmod, and VanLeer constraints. The Courant number for all schemes is 0.2, except for rhoCentralFoam VanLeer, for which the best calculation option for the Courant number of 0.1 is given.

It follows from the graphs that the second-order approximation schemes with VanLeer limiters and the first-order minmod schemes introduce a large number of oscillations in the solution and turn out to be far from the standard. The upwind first-order scheme turns out to be strongly dissipative and smoothens the

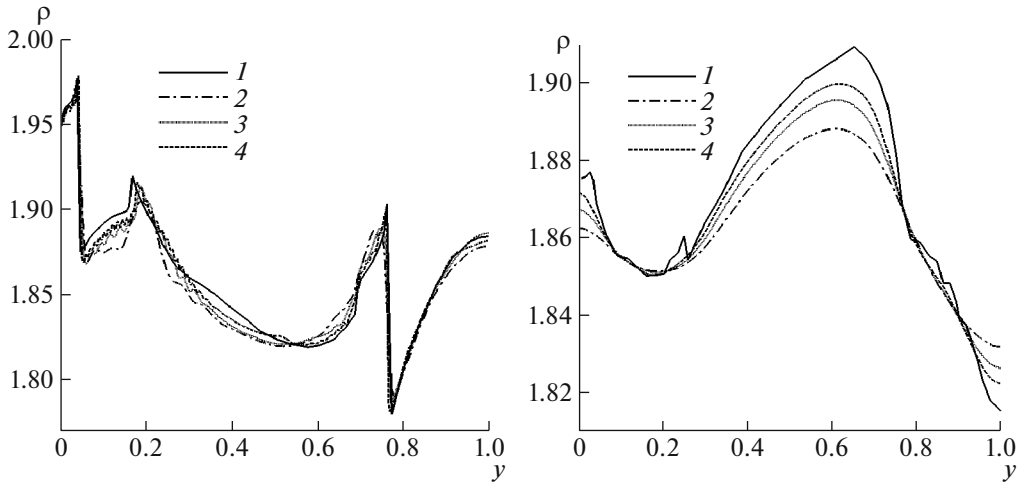

Fig. 5. Grid convergence. Density ρ along lines *3* ($x = 0.52$, left figure) and *5* ($x = 1.65$, right figure) $\alpha = 0.2$, $\mathrm{Sc} = 0$ for spatial grids with steps $h = 1/400$ (*2*), $1/800$ (*3*), $1/1600$ (*4*); (*1*) is the reference solution.

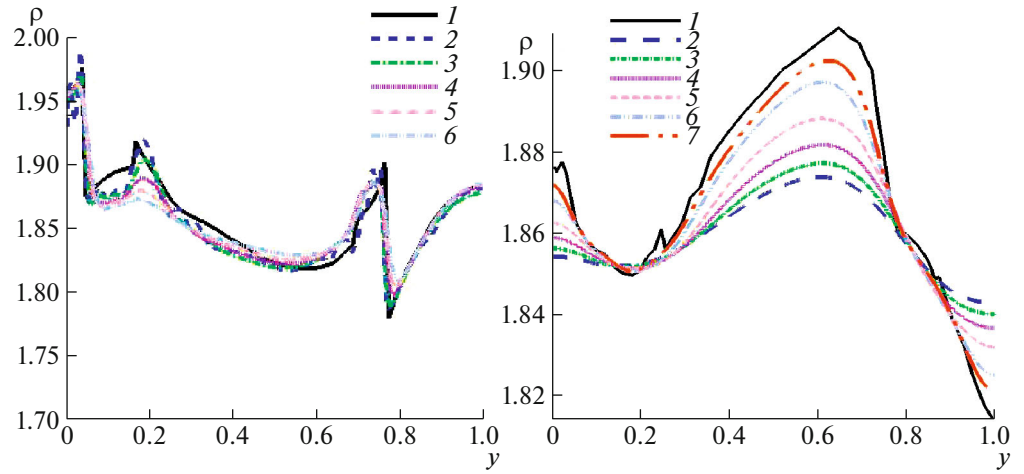

Fig. 6. Convergence of parameter α. Density ρ along lines *3* and *5*, grid $h = 1/400$. (*1*) reference solution, (*2*) $\alpha = 0.5$, (*3*) $\alpha = 0.4$, (*4*) $\alpha = 0.3$, (*5*) $\alpha = 0.2$, (*6*) $\alpha = 0.1$, (*7*) $\alpha = 0.05$.

solution much more than the first two methods, and more than the QGD algorithm, whose difference scheme also has the first-order of approximation in space. The general structure on the specified grid is best drawn by the QGD method; see Fig. 3.

Figure 8 shows the density graphs ρ along lines *3* and *5* on the grid $h = 1/400$ for the same solvers. For comparison, the graphs are supplemented with the result obtained for the QGD algorithm with $\alpha = 0.05$ and $\mathrm{Sc} = 0$. These plots show that the profiles obtained by the upwind and QGD methods turn out to be close at large values of the QGD dissipation coefficient $\alpha = 0.5$. For small values of this coefficient of $\alpha = 0.1$ or 0.05, the results of the QGD calculations are close to the results obtained by the schemes of the second order of accuracy with the VanLeer limiter. This agrees with the estimate of the order of approximation of the QGD schemes, which has the form $O(\alpha h)$ at $\alpha > \alpha_{\min} > 0$, where $\alpha_{\min}$ is a certain minimum coefficient that ensures the stability of the numerical algorithm.

RESULTS AND DISCUSSION

Based on the example of solving a test problem on the unsteady interaction of a vortex flow with a shock wave, we analyzed the features of the QGD algorithm included in the OpenFOAM platform, together

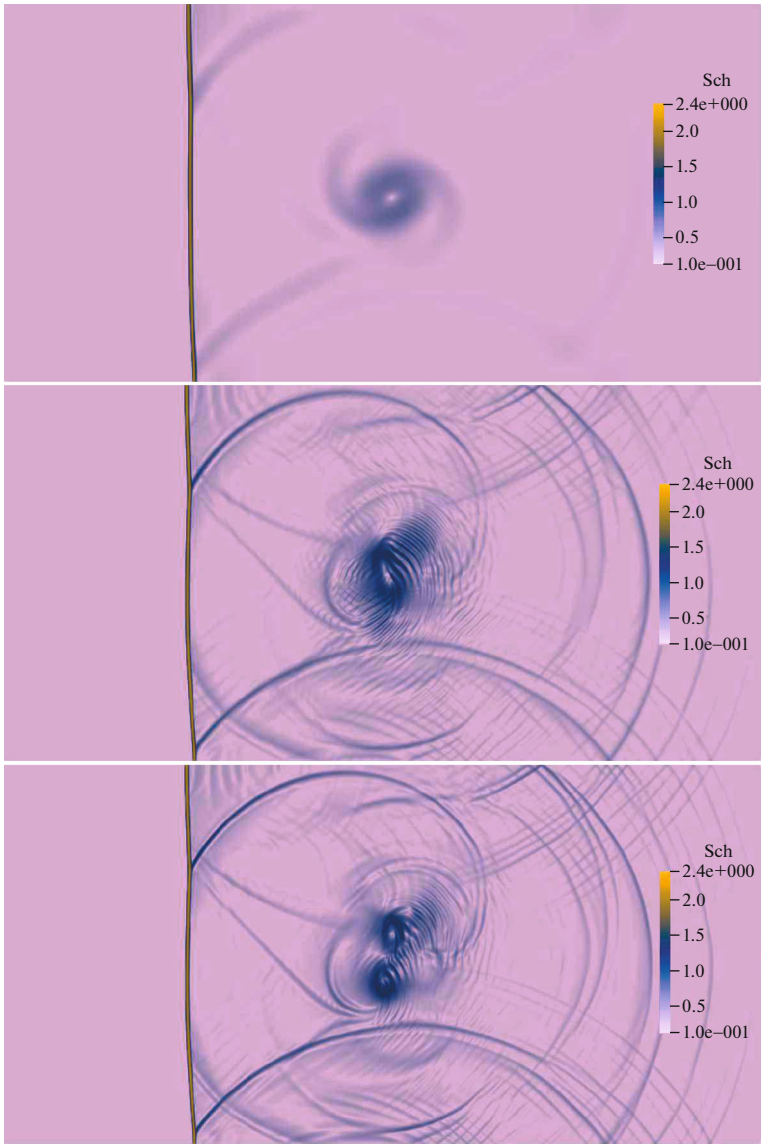

Fig. 7. $t = 0.7$. Grid $h = 1/400$, upwind, minmod, and VanLeer constrained solvers (top to bottom).

with three other computational cores included in the same platform: variants of the rhoCentralFoam solver with VanLeer second-order accuracy limiters and first-order limiters of the minmod and upwind order of accuracy. A detailed formulation of the problem and a comparison of the calculation results with data from other methods are given.

It was shown that the QGD algorithm solves the problem and the results of calculations converge monotonically to the solution considered as the reference solution, when the spatial grid is refined. As the dissipation coefficients decrease to the stability limit of the algorithm, its accuracy also increases. At small values of the dissipative coefficients, the results of the QGD calculations are close to the results obtained by the scheme of the second-order of accuracy, and at large values, they are close to the results of calcu-

Table 3. Calculation time in seconds for 1000 steps on an 800 × 400 grid

QGDFoam	QGDFoam reduced	rhoCentralFoam VanLeer	rhoCentralFoam minmod	rhoCentralFoam upwind
18.3	13.8	10.9	10.0	6.2

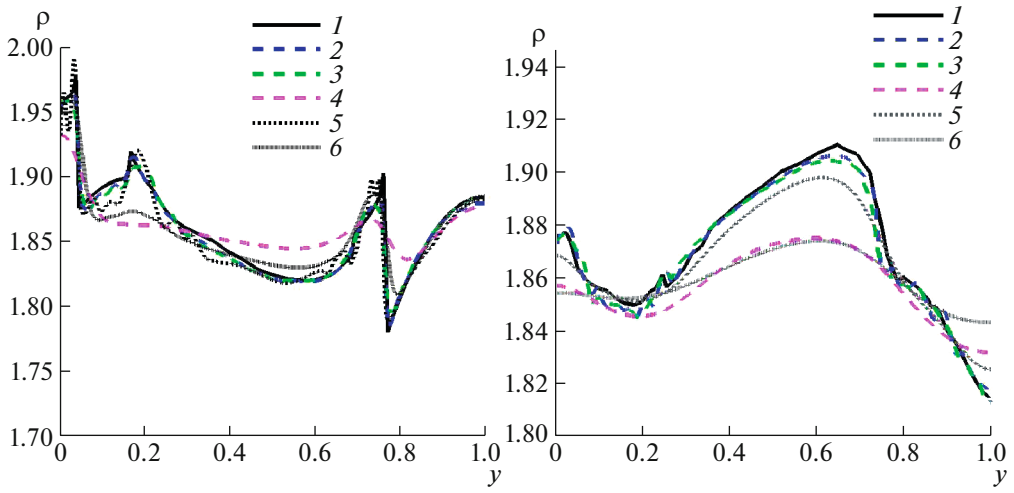

Fig. 8. Density ρ along lines *3* and *5*, grid $h = 1/400$, (*1*) reference solution, (*2*) VanLeer with Courant number Co = 0.1, (*3*) minmod, (*4*) upwind, (*5*) QGD, $\alpha = 0.1$, Sc = 0, (*6*) QGD, $\alpha = 0.5$, Sc = 0.

lations by the scheme of the first-order of accuracy with upwind differences. A rather simple adjustment of the dissipative coefficients in the QGD algorithm allows us to tune it to obtain a solution with the required accuracy.

To evaluate the computational efficiency of the methods, Table 3 compares the computation time of the task when it is implemented on one processor of the K-100 computer system. An example of solving the problem in 1000 time steps on a grid $h = 1/400$, i.e., on a grid with 800 × 400 points, was considered. The results presented are obtained after averaging the calculation time over five calculation options for each scheme. The calculation times for QGDFoam, QGDFoam reduced, rhoCentralFoam VanLeer, rhoCentralFoam minmod, and rhoCentralFoam upwind are presented.

The QGDFoam algorithm is the most time consuming algorithm, due to the computational complexity of the calculation τ terms that include mixed spatial derivatives. In the QGDFoam reduced version, these mixed derivatives are disabled, and the algorithm is less computationally consuming. At the same time, in this problem, the calculation results for both versions of the algorithm turn out to be quite close to each other. Variants of rhoCentralFoam with the specified constraints are more efficient in terms of calculation time; however, the accuracy of the solution and the qualitative form of the obtained density distributions turn out to be low.

Thus, this study shows that the difference scheme of the first order of approximation, built based on QGD equations, with an appropriate selection of numerical coefficients in artificial dissipative terms, solves the problem sufficiently accurately. The obtained results show that in order to increase the accuracy of the calculations, the transition to high-order approximation algorithms can be supplemented by the use of first-order approximation algorithms with highly nonlinear and finely tuned dissipative terms.

CONFLICT OF INTEREST

The authors declare that they have no conflicts of interest.

REFERENCES

1. A. V. Rodionov, “Simplified artificial viscosity approach for curing the shock instability,” Comput. Fluids **219**, 104873 (2021). https://doi.org/10.1016/j.compfluid.2021.104873
2. 5th International Workshop on Hight-Order CFD Methods. https://how5.cenaero.be/.
3. T. G. Elizarova, *Quasi-Gas Dynamic Equations* (Nauchnyi Mir, Moscow, 2007; Springer, Berlin, 2009). https://doi.org/10.1007/978-3-642-00292-2

4. T. G. Elizarova, "Time averaging as an approximate technique for constructing quasi-gasdynamic and quasi-hydrodynamic equations," Comput. Math. Math. Phys. **51** (11), 1973–1982 (2011). https://doi.org/10.1134/S0965542511110078
5. M. V. Kraposhin, E. V. Smirnova, T. G. Elizarova, and M. A. Istomina, "Development of a new OpenFOAM solver using regularized gas dynamic equations," Comput. Fluids **166**, 163–175 (2018). https://doi.org/10.1016/j.compfluid.2018.02.010
6. A. Kurganov and E. Tadmor, "New high-resolution central schemes for nonlinear conservation laws and convection-diffusion equations," J. Comput. Phys. **160** (1), 241–282 (2000). https://doi.org/10.1006/jcph.2000.6459
7. M. Elghorab, V. C. Madhav Rao, and J. X. Wen, "Evaluating the capability of the flux-limiter schemes in capturing the turbulence structures in a fully developed channel flow," Int. J. Aerosp. Mech. Eng. **12** (2), 175–181 (2018). https://doi.org/10.5281/zenodo.1315963
8. I. Yu. Tagirova and A. V. Rodionov, "Application of artificial viscosity for suppressing the carbuncle phenomenon in Godunov-type schemes," Math. Models Comput. Simul. **8** (3), 249–262 (2016). https://doi.org/10.1134/S2070048216030091